Supporting Information

Cyclic transformation of stable/metastable nucleic acid structures enables dynamic monitoring of ATP in living cells

*Ming-Li Su[a #], Jun Yang[a, #], Wei-Guo Yang[a, #], Zhuo-Xin Ye [c], Rui-Wen Wang[a], Jia-Min Qin[a], Da-Qian Song[c], Ruo Yuan[a], Pin-Yi Ma [c], Ying Zhuo[a], ChaoYong Yang [b], Wen-Bin Liang[a, *]*

[a] Key Laboratory of Luminescence Analysis and Molecular Sensing (Southwest University), Ministry of Education, College of Chemistry and Chemical Engineering, Southwest University, Chongqing, 400715, China.

[b] Institute of Molecular Medicine, Shanghai Key Laboratory for Nucleic Acid Chemistry and Nanomedicine, State Key Laboratory of Oncogenes and Related Genes, School of Medicine, Shanghai Jiao Tong University, Shanghai, 200127, China.

[c] College of Chemistry, Jilin Province Research Center for Engineering and Technology of Spectral Analytical Instruments, Jilin University, Changchun, 130012, China.

Table of Contents

Chemicals and materials. $MgCl_2 \cdot 6H_2O$, ATP, adenosine diphosphate (ADP), and adenosine monophosphate (AMP) was purchased from KKL MED Inc. Guanosine triphosphate (GTP), uridine triphosphate (UTP) and cytidine triphosphate (CTP) were obtained from Geneview Biotechnology Company. RNA transfection was performed using liposomal transfection reagent (Lipofectamine 3000, Thermo Fisher Scientific, New York, USA). All the oligonucleotides used in this experiment (Table S1) were offered by Shanghai Sangon Biological Engineering Technology and Services Company, Ltd. (Shanghai, China). 4-(2-Hydroxyethyl)-1-piperazineethanesulfonic acid (HEPES pH=7.4) buffer was prepared with 40 mM HEPES, 100 mM KCl and 5 mM Mg^{2+}. (4-((2-Hydroxyethyl) (methyl) amino) -benzylidene)-cyanophenylacetonitrile (HBC) was prepared through a synthetic procedure outlined in documented literature[16]. Subsequently, it undergoes dilution to a concentration of 1 mM in dimethyl sulfoxide (DMSO), followed by further dilution with HEPES to reach the desired working concentration. Ultra-pure water, characterized by a resistivity of 18 MΩ·cm, is subjected to purification through water purification system.

Apparatus. All fluorescence responses were obtained through testing with an F-7000 instrument (Hitachi, Tokyo, Japan) with an excitation slit of 5 nm and an emission slit of 10 nm, respectively. Cellular imaging was conducted using total internal reflection fluorescence microscopy (TRIFM) and ultra-high speed and super resolution real time dynamic imaging system (SpinSR, Olympus, Tokyo, Japan). All the buffer solutions used in the experiments were calibrated with pH device (LeiCi, Shanghai, China). Isothermal titration calorimetry date was obtained from MicroCal ITC200 (Malvern Panalytical Inc, MA, USA)

RNA Structure Simulation and Docking Experiment. To further investigate the collaborative binding of HBC and ATP with ATP-EF and ATP-CT for understanding of the dynamic analysis mechanisms, we employed molecular docking application with AutoDock Vina in this study. The 3D model of ATP was procured from Zinc (ZINC4261765), whereas the simulation of the 3D structures of RNA emanated from the Xiao Lab**.** (http://biophy.hust.edu.cn/new/3dRNA/create). Finally, all 3D structures are processed through Pymol to generate PDB files. The free energies of the nucleic acid secondary structures were estimated using the RNAeval module in the ViennaRNA Package, together with predictions from NUPACK. The RNAeval module calculates the thermodynamic free energy of a specified RNA secondary structure based on the input nucleic acid sequence and its corresponding secondary structure.

Oligonucleotides Probe Design and Reaction Principle. The formation dynamics of nucleic acids structures are fundamentally governed by thermodynamic equilibria. When the Gibbs free energy difference (ΔG) between the alternative nucleic acid conformation falls below a threshold, it can be assumed that the nucleic acids adopt multi-conformations coexistence states. By modulating non-functionalized sequence domains while preserving ligand-binding competence of the aptamer, we implement in-silico optimization to rationally engineer aptamer probes, thereby achieving their programmable spatial structures. Two nucleic acid structural configuration regulation mechanisms, "equilibrium fluctuations" and "conformational transitions", were developed in this experiment based on the cyclic transformation of nucleic acid stable/metastable structure respectively that synergize three-dimensional topology engineering with free energy landscape manipulation, thereby further constructing a dynamic equilibrium network, in which probe molecules naturally oscillate between multiple conformations.

In Vitro Fluorescence Characterization. All fluorescent signals were excited at 485 nm with an excitation slit width of 5 nm and an emission slit of 10 nm, and the signal intensity at 530 nm was collected. FL kinetic signal acquisition was also conducted under the same experimental conditions. In evaluating the dynamic analysis performances, the APyrase was added to simulate the process of ATP depletion and degradation in *vivo*, and the enzyme was inactivated by placing the enzyme at 65°C for 20 min after the measurement of FL signals. Then a certain amount of the reaction substrate as well as HBC were added to maintain the same concentration before and after the reaction. And then, the FL signals were measured, respectively. All of these experimental processes were repeated for several times (n>3).

Pre-processing and Preparation of Samples. All of the oligonucleotides were centrifuged at 4 °C for 15 minutes and subsequently dissolved in DEPC treated water, that were diluted to the working concentration using HEPES buffer with 5 mM Mg^{2+}. Before using, the oligonucleotides were heated to 65 °C and maintained for 10 minutes, followed by a slow cooling to 25 °C within one hour, facilitating the formation of the corresponding three-dimensional structure. HBC was subsequently dissolved in DMSO and diluted to establish stock solution (1 mM). Furtherly, it was diluted with HEPES buffer for meticulous dilution to achieve the exact concentration necessary for subsequent nucleic acid reactions. To prevent alterations in the ionic strength of the reaction system upon the addition of reaction components, ATP, ADP, AMP and similar compounds are dissolved in HEPES buffer.

Cell culture and biological sample analysis. Hela and MCF-7 cells were cultured in DMEM medium supplemented with 10% fetal bovine serum and 5% penicillin-streptomycin, maintaining at 37°C with 95% humidity and 5% carbon dioxide. Following nucleic acid annealing, the introduction of HBC and liposomes 3000 was added, and the resulting mixture was diluted to a predetermined volume with DMEM. This diluted solution was then added to a culture dish for the transfection of 8 hours. After careful washing with PBS, the cells were stained separately with 70 μL Hoechst 33342 and Mito Tracker Red CMXRos for 15 mins. Lipofectamine 3000 from Thermo Fisher Scientific was used as the transfection reagent. Briefly, the corresponding proportion of Lipofectamine 3000 was mixed with the nucleic acid substrates and 2 μM HBC, followed by thorough mixing and incubation at room temperature for 20 min to form the transfection complexes. The resulting mixture was then added to cells at approximately 50–60% confluency. After 4 h of transfection, the culture medium was replaced with fresh medium prior to subsequent dynamic imaging experiments. Time-lapse imaging experiments were performed using a super-resolution spinning-disk confocal microscope equipped with a live-cell incubation system. For fluorescence acquisition, the 488 nm laser channel was operated at 50% laser power with an exposure time of 200 ms, while the 561 nm laser channel was operated at 25% laser power with an exposure time of 100 ms.

Intracellular ATP dynamics detection

After transfection of three ATP probes (ATP-EF, ATP-CT, and FISHER) into cells, fluorescence signals were collected using a confocal laser scanning microscope under

the 485 nm excitation channel and compiled into videos. Subsequently, regions of interest (ROIs) within individual cells were selected for quantitative fluorescence intensity analysis, as shown in **Supporting Video**.

Free energy simulation and reaction constant calculation. Predicting the nucleic acid conformational conversion rate constant *k* is crucial for understanding its dynamic behavior upon ligand binding. We first calculated the free energies of the nucleic acid in different states using RNAfold and NUPACK for structural free energy, and AutoDock Vina for ligand binding free energy. The total free energy difference driving the conformational change was defined as

$$\Delta G_{conversion} = \Delta G_{bound\_total} - \Delta G_{initial} = (-33.40) - (-26.44) = -6.96\ kcal/mol$$

Where $\Delta G_{initial}$ is the free energy of the initial unbound nucleic acid, and ΔG_{bound_total} is the combined free energy of the ATP-bound nucleic acid complex.

Based on the classical thermodynamic relation:

$$\Delta G = -RT\ ln\ k$$

The rate constant *k* is given by:

$$k = e^{\left(\frac{-\Delta G_{conversion}}{R \times T}\right)} \approx 8.05 \times 10^{4}\ s^{-1}$$

where *R*=1.987×10⁻³ kcal/(mol·K) and T = 310.15 K (37°C). ATP-CT was treated in the same way.

Table S1: Nucleic acid sequences used in the experiments

Name	Sequence from 5' to 3'
ATP-EF	CGG CAG GCA CUG GCG CCG ACC GUA GUG GUG UGU GUG UGG GUC CAA UCG UGG CGU GUC GGC CUG CUU
ATP-EF-1	CGG CAG GCA CUG GCC CGG ACG UAG UGG UGU GUG UGU GGU CCC AAU CGU GGG UGU CGG CCU GCU U
ATP-CT	CCA AUC CAA UCG UGG CGU GUC GGC CUG CUU CGG CAG GCA CUG GCG CCG AUU GGG GGG UGG AAG AAA CUG UGG CAC UUC GGU GCC AGC CCC
ATP-CT-1	CCC AAU CCA AUC GUG GCG UGU CGG CCU GCU UCG GCA GGC ACU GGC GCC GAU UGG GGG GUG GAA GAA ACU GUG GCA CUU CGG UGC CAG CCC
N-1	UUC CCC AAC AAU GGC ACC GGC UUA GGG GAG GGG ACC AAU CGU GGC GUG UCG GCC UGC UUC GGC AGG CAC UGG CGC CGC UCC
N-2	UCC CCA ACA AUG GCA CCG GCU UAG GGG AGC AAU CGU GGC GUG UCG GCC UGC UUC GGC AGG CAC UGG CGC CGG GGG A
N-3	UCC CCA ACA AUG GCA CCG GCU UAG GGG CCC AAU CGU GGC GUG UCG GCC UGC UUC GGC AGG CAC UGG CGC CGG GGG A
N-4	UUC CCA ACA AUG GCA CCG GCU UAG GGG GGG AAU CGU GGC GUG UCG GCC UGC UUC GGC AGG CAC UGG CGC CGC CCA
Pepper	UGU CCC AAU CGU GGC GUG UCG GCC UGC UUC GGC AGG CAC UGG CGC CGG ACA AGA
FISHER-FAM	AGAGAACCTGGGGGAGTATTGCGGAGGAAGGT
FISHER-BHQ1	CTCCGCAACCCAGGTTCTCT

Life Molecule Application Expansion

In addition to systematically rationalizing the potential reasons of the insufficient fluorescence signal amplification, we further performed a comprehensive comparative assessment of three distinct design strategies for the NADH nucleic acid sequence. Weak base-pairing elements within the locking region are necessary to the terminus of the nucleic acid sequence. Through base-pairing–induced spatial distortion, the recognition region of HBC was partially perturbed, thereby weakening interstrand interactions and consequently reducing background signals. With this strategy, we construct a new substrate for NADH dynamic analysis named as N-2 (Fig. S1B). Based on computational simulations, the recognition region and the signal region were designed to adopt metastable states. Under this condition, the nucleic acid structure was prevented from existing in a single stable conformation and instead populated multiple coexisting conformations that was essential to generate target-induced conformational transformation. With this strategy, we construct a new substrate for NADH dynamic analysis named as N-3. The locking capability of the interaction segment between the recognition region and the signal region was enhanced by introducing additional base pairs, thereby suppressing undesired signal leakage. This designed sequence was named as N-4. The feasibility of each design was subsequently evaluated, and sequences exhibiting higher SNB values were screened for further construction of the standard calibration curve. As shown in Fig. S1A, N-2 exhibited the highest relative fluorescence change. On this basis, the fluorescence intensity responses to varying concentrations of the target were investigated, and the corresponding linear relationship was established (Fig. S1C and D).

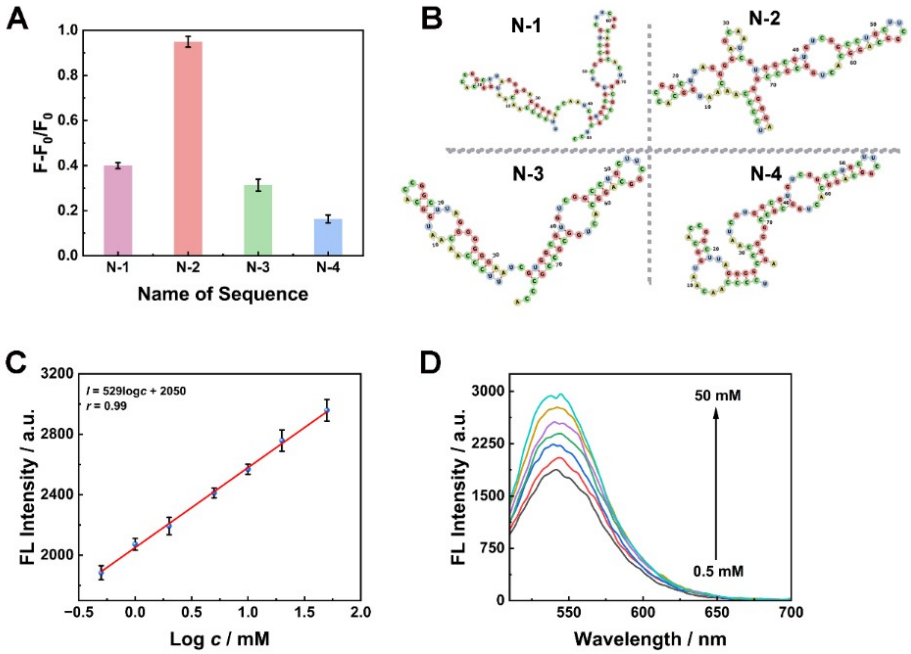

Fig. S1 (A) Schematic illustration of the feasibility of different structural NADH signal probes, evaluated by the relative fluorescence response. (B) Two-dimensional structural configurations of the four designed NADH probes. (C) Linear relationship between NADH concentration and fluorescence intensity with regression fitting. (D) Fluorescence emission spectra of the probe at varying NADH concentrations.

Thermodynamic calculation and simulation

The corresponding free energies and docking binding energies of nucleic acids and small molecules were calculated for the configurations of ATP-EF and ATP-CT both before and after binding. Using the relationship $\Delta G = -RT\ln k$, the reaction rate constants for each step were determined. These calculations provide a more precise thermodynamic explanation for the feasibility of nucleic acid conformational changes.

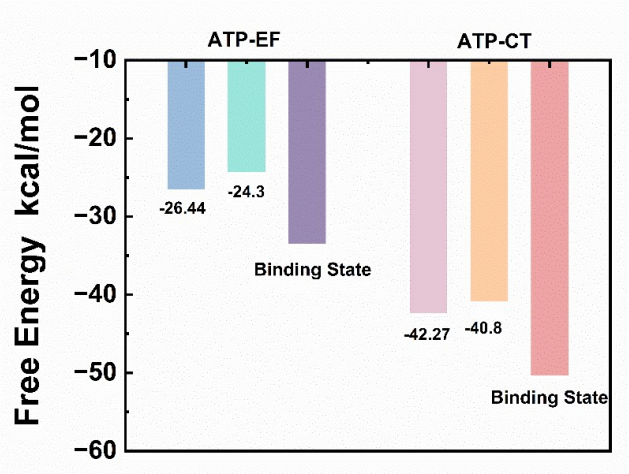

Fig. S2 Analysis of free energy of nucleic acid conformations.

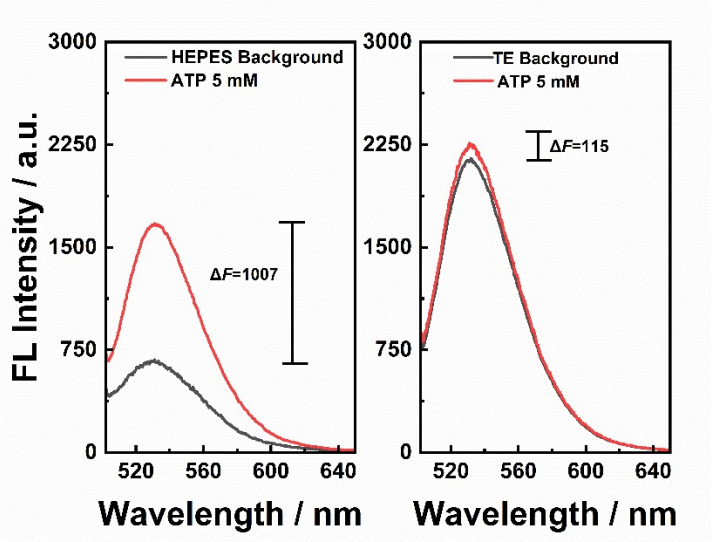

Fig. S3 Fluorescence signal response of ATP (5 mM) in different buffer (HEPES buffer with 40 mM HEPES, 100 mM KCl and 5 mM Mg^{2+} and Tris-EDTA buffer with 10 mM Tris, 1 mM EDTA, 5 mM Mg^{2+}

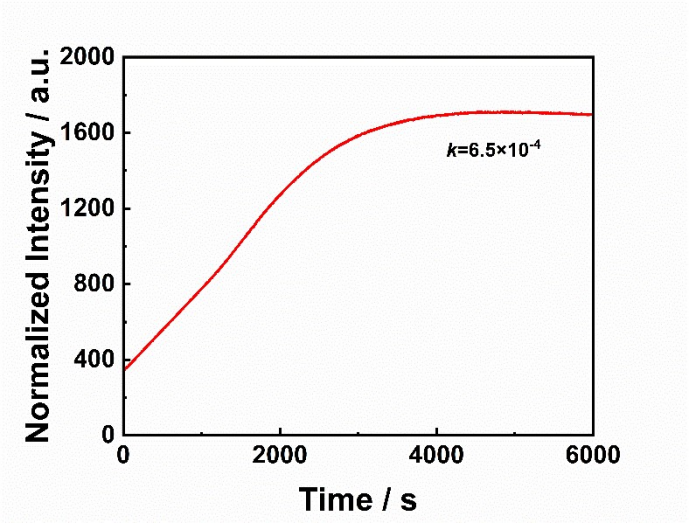

Fig. S4 The fluorescence characterization of ATP molecular concentration changes in *vitro* using the ATP-CT.

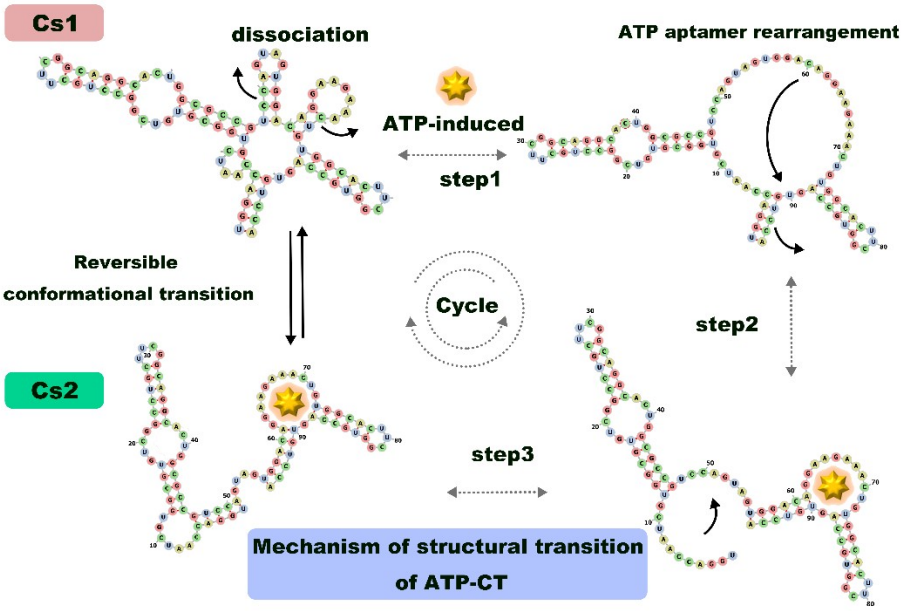

Fig. S5 Schematic mechanism of the allosteric reaction induced by ATP-CT small-molecule binding.

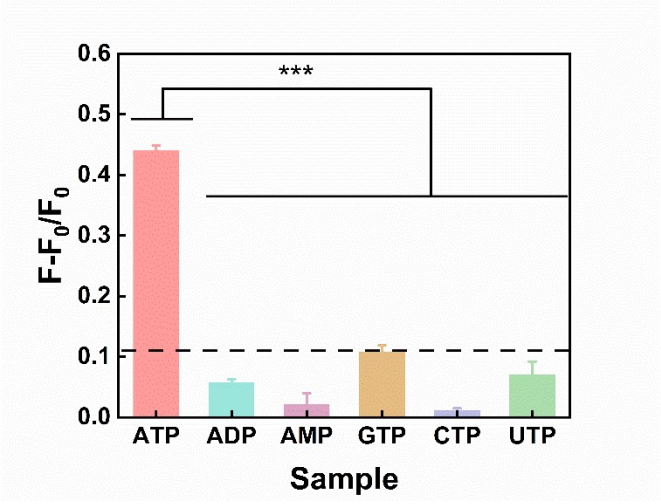

Fig. S6 Evaluation of the specific recognition ability of ATP-CT probe. ATP and the other interfering species were used at the same concentration of 1 mM.

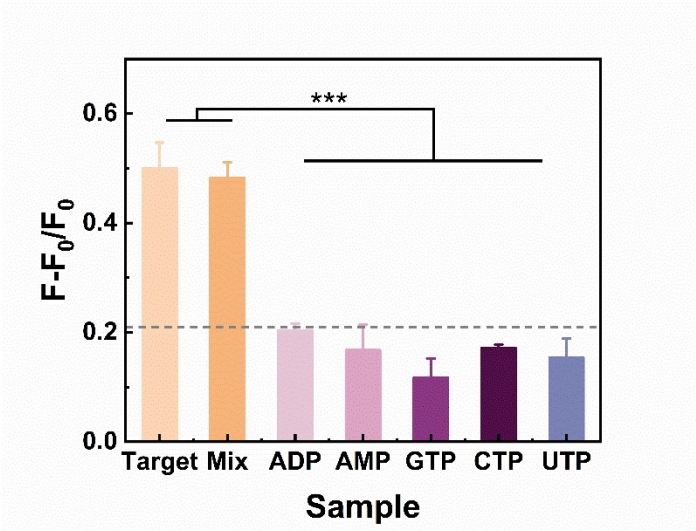

Fig. S7 Evaluation of the specific recognition ability of ATP-EF probe. ATP and the other interfering species were used at the same concentration of 100 mM.

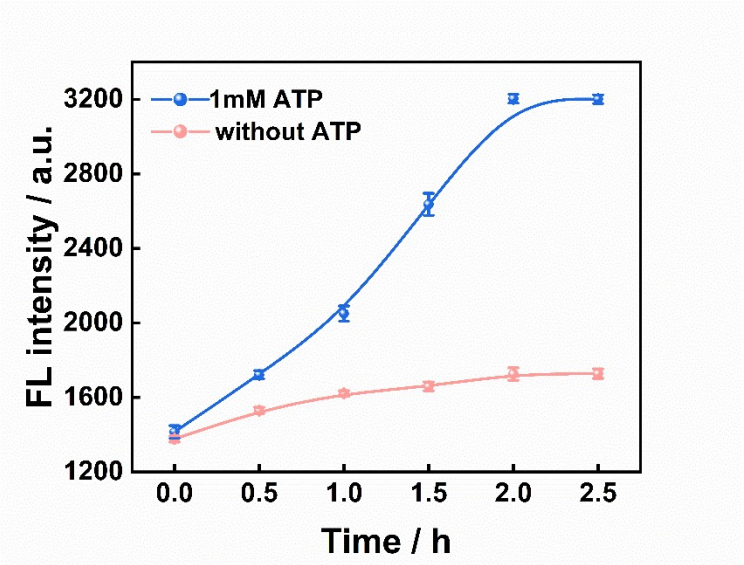

Fig. S8 Optimization of hybridization time in ATP-CT analysis environment.

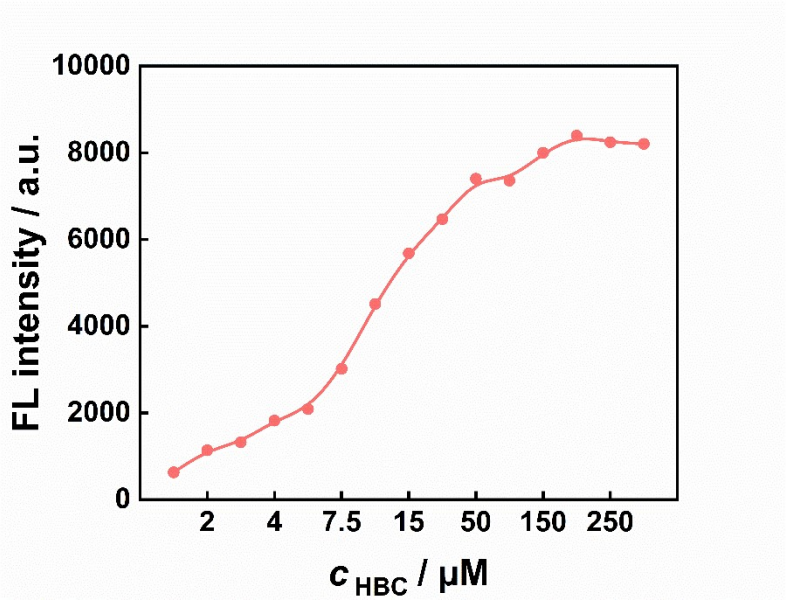

Fig. S9 Relationship between HBC concentration and fluorescence signal.

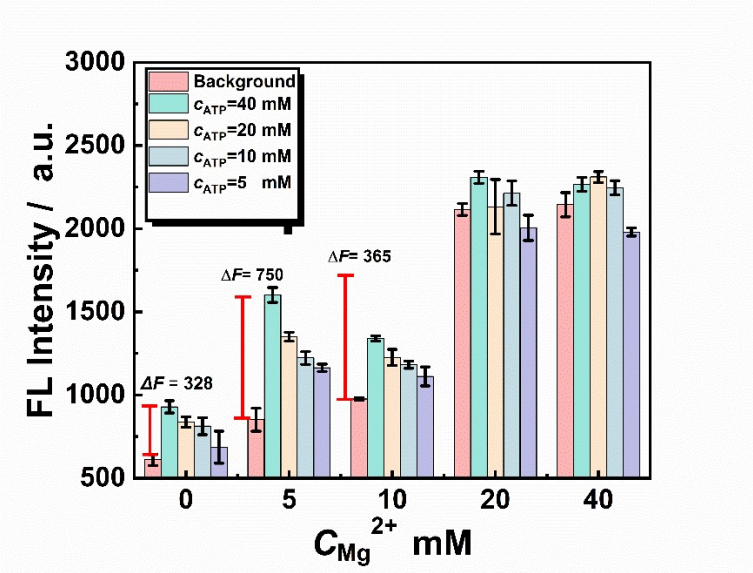

Fig.S10 Optimization of Mg^{2+} concentration in ATP-EF analysis environment.

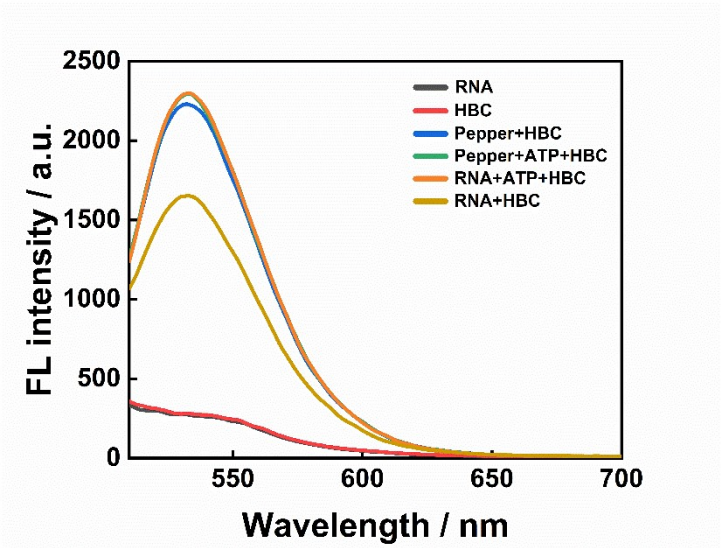

Fig. S11 Fluorescence signal feasibility verification.

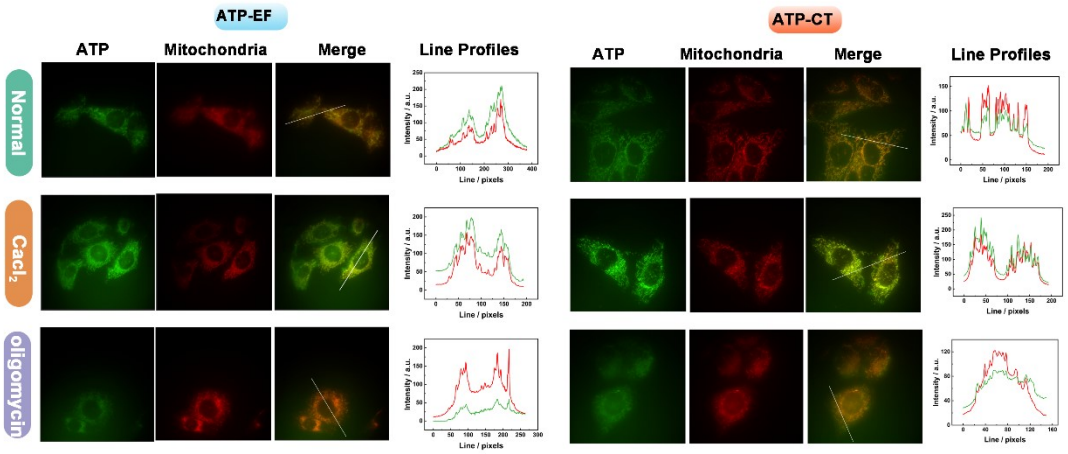

Fig. S12 Line profile analysis of ATP fluorescence signals around mitochondria and ATP expression levels. (Green line represents ATP, Red line represents mitochondria)